AIAA JOURNAL
Vol. 34, No. 9, September 1996

Acoustic Response of Droplet Flames to Pressure Oscillations

C. H. Sohn* and S. H. Chung†
Seoul National University, Seoul 151-742, Republic of Korea
and
J. S. Kim‡ and F. A. Williams§
University of California, San Diego, La Jolla, California 92093-0411

The acoustic pressure response of spherical H_2/liquid oxygen droplet flames is studied by the premixed-flame regime of activation-energy asymptotics to examine acoustic instability mechanisms in liquid-propellant rocket engines. Depending on the diameters of the droplets, the combustion condition is classified as near-equilibrium or near-extinction, and the acoustic pressure response for each condition is determined for a wide range of the acoustic frequency. Compared with the results previously obtained for strained diffusion flames, the reaction sheet of the droplet flame is found to exhibit a behavior similar to that of strained diffusion flames, in that the reaction sheet moves toward the oxidizer boundary, at which the mass flux of the oxidizer is greater, to balance the high reactivity during the period of high acoustic pressure. Oscillations of the reaction sheet also give rise to an additional attenuation mechanism, associated with reduction of the reaction-surface area, thereby resulting in a much smaller response of the heat-release rate for droplet flames than that for strained diffusion flames.

Nomenclature

B = frequency factor (s^{-1}) for rate of fuel mass consumption
c_p = specific heat at constant pressure
D = mass diffusion coefficient
D_T = thermal diffusivity
Da = Damköhler number
E = activation energy for rate of fuel consumption
G, Z = coupling functions defined in Eq. (4)
h, h'' = nondimensional heat release rates as defined in Eqs. (37) and (38)
L = latent heat of evaporation, made nondimensional through division by Q^*
Le = Lewis number
m = nondimensional mass flux, $\equiv \rho u x^2$
p = pressure
Q = heat released per unit mass of fuel consumed
q = nondimensional heat release, $\equiv Q^*/c_p^* T_\infty^*$
R = universal gas constant
r = radial coordinate
T = temperature
t = time coordinate
u = radial velocity
w = nondimensional rate of fuel mass consumption per unit volume, defined in Eq. (10)
x = nondimensional radial coordinate defined in Eq. (3)
Y = mass fraction
β = Zel'dovich number defined in Eq. (20)
γ = ratio of the specific heat at constant pressure to that at constant volume
θ = normalized temperature defined in Eq. (1)
ρ = density
σ = stoichiometric mass ratio of oxidizer to fuel
τ = nondimensional time defined in Eq. (3)
ω = acoustic frequency

Subscripts

d = droplet
e = extinction condition
F = fuel
f = conditions at the reaction sheet
g = gas
i = conditions at the initial state
l = liquid
O = oxidizer
s = conditions at the droplet surface
x = partial derivative with respect to x
∞ = conditions at infinity, far from the droplet

Superscripts

$\bar{}$ = mean field
$\tilde{}$ = oscillatory field
$\hat{}$ = partial derivative of the mean field with respect to x_f
$\check{}$ = total derivative of the mean-field variable at x_f with respect to x_f
$*$ = dimensional quantity

Received Oct. 7, 1995; revision received May 9, 1996; accepted for publication May 22, 1996.

*Graduate Student, Department of Mechanical Engineering.
†Professor, Department of Mechanical Engineering. Member AIAA.
‡Assistant Research Scientist, Center for Energy and Combustion Research.
§Professor, Center for Energy and Combustion Research. Fellow AIAA.

Introduction

ACOUSTIC instabilities in liquid-propellant rocket engines, in which oscillations of the chamber pressure corresponding to the acoustic eigenmodes of the cavity are amplified mainly through interactions with combustion, enjoy a long history of scientific and technological study.[1,2] The steady droplet-flame model is one that has been adopted as a microscopic flame model for turbulent spray flames inside rocket engines for describing both steady operation and acoustic instability. Although this model has met with some success in predicting steady performances of rockets, the steady approximation is appropriate for acoustic instabilities only when the characteristic acoustic time is much larger than the characteristic diffusion time of droplet flames. Because this last condition is not satisfied in real rockets, Strahle[3] analyzed acoustic response of unsteady droplet combustion in the forward stagnation-point region, calculating the unsteady accumulation that produces impedance of the droplet-flame response to acoustic waves. However, the influences of finite-rate chemistry were not included in his work, and comparison of his work with our previous analysis[4] on acoustic response of strained diffusion flames near extinction has shown that the effects of finite-rate chemistry can lead to an order-of-magnitude increase in amplification contributions because the dominant nonlinear term in combustion processes arises from finite-rate chemistry.

Use of detailed chemical kinetics makes analyses exceedingly complicated, so that, as a mathematical model, activation-energy

asymptotics (AEA) can be employed.[5] A recent analysis for hydrogen–air flames[6] verified that AEA does provide a qualitatively reasonable structure for H_2–O_2 flames. In the limit of asymptotically large Zel'dovich number β (a ratio of the effective activation energy to the thermal energy), chemical reaction is confined to an asymptotically thin layer with thickness of order β^{-1} compared to the thickness of the diffusive transport zone, and thus the characteristic time for reaction is much shorter, by a factor of order β^{-2}, than the characteristic diffusion time. Particularly for flames near extinction, the characteristic diffusion time of laminar diffusion flames can be estimated from the extinction strain rate to be in the range of 10^{-3}–10^{-4} s, which turns out to be of the same order as the characteristic acoustic time given by the reciprocal of the acoustic frequency. Therefore, the analysis can be performed in a distinguished limit, in which the timescale of the acoustics is comparable to that of the diffusive transport, such that the outer convective–diffusive layer is modified to include the unsteadiness caused by the acoustics, whereas the inner reactive layer remains quasisteady. The effect of finite-rate chemistry then will influence the unsteady flame response only through the instantaneous matching conditions at the reaction sheet. The effect that was not included in the work of Strahle[3] is the influence of this matching with decreasing Damköhler number as the flamelets approach extinction.

Recently, AEA flame analysis has been developed to calculate acoustic responses of solid- and liquid-propellant flames.[4,7] In particular, a strained laminar diffusion flame[4] was employed as a model flamelet in liquid-propellant rockets to predict responses of the burning rate to the imposed acoustic pressure oscillations in terms of their magnitude and phase. It was shown that such responses become very sensitive to the acoustic oscillations as the mean flame approaches extinction. In the present paper, the analysis of Kim and Williams[4] is extended to combustion of subcritical liquid oxygen (LOX) droplet burning in stagnant gaseous fuel, typically hydrogen to provide the phase and amplitude relations needed for use in amplification expressions.

Although droplet combustion in turbulent flames occurs in convective environments, results of the present analysis, combined with those for strained diffusion flamelets, will be relevant to convective droplet flamelets. Convective droplet flames burn most vigorously in the forward stagnation-point region of the droplets. The characteristics of combustion in that region can be qualitatively predicted from those of spherical droplet flames and strained diffusion flames because fluid mechanical properties of stagnation-point flows are similar to those of counterflows, whereas multiphase transport processes resemble those of droplet flames. Results of acoustic responses in these elementary flamelets enable us to identify types of flamelets that produce greater amplification contributions to acoustic instabilities. Recently, results of our strained diffusion-flamelet model were applied to explain an empirical correlation that shows where instability boundaries of the LOX/RP-1 rocket lie.[8]

Attention is focused on linear instabilities of acoustic waves, so that the flame response can be expressed as a linear combination of the pressure response and velocity response, each of which can be calculated separately by assuming that the flamelet is located either at a pressure node or at a velocity node. However, the present analysis is restricted to the pressure response only. The increase of the burning rate in the absence of mean relative convection is dependent on the absolute magnitude of the acoustic velocity, so that the frequency of the velocity response is twice that of the imposed acoustic frequency. The velocity response thus does not provide a linear amplification of acoustic waves. In addition, the amplitude of acoustic pressure is assumed to be spatially uniform because the characteristic wavelength is much larger than the characteristic droplet-flame diameter.

Flame-Structure Analysis

Conservation Equations

A schematic diagram of droplet flames considered here is shown in Fig. 1. To simplify the problem, a number of assumptions are made. Oxidizer, vaporized from the droplet, and fuel are assumed to be ideal gases. The Soret and Dufour effects are neglected. Viscous dissipation also is neglected because the Mach number in the droplet flame is much smaller than unity. Because oxygen is the only material transported in the region between the reaction sheet and the droplet surface (the products there having their diffusion and convection cancel exactly), the Lewis number in zone I of Fig. 1 is unity,[9] whereas the Lewis number for fuel in zone III is assumed to be constant but not necessarily unity. Finally, the thermal diffusivity multiplied by the density is taken to be proportional to T^a, where a is a constant.

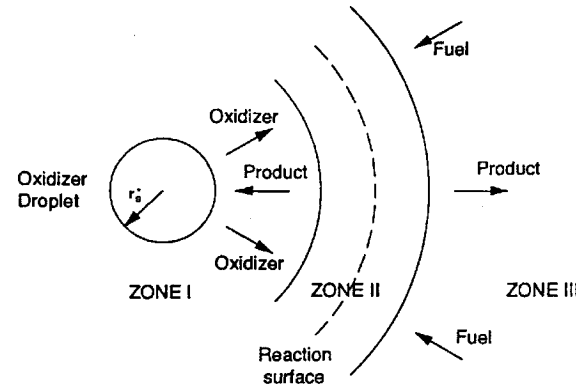

Fig. 1 Schematic diagram of oxygen droplet combustion in a gaseous fuel atmosphere. Zones I and III, unsteady convective-diffusive layer (chemically frozen) and zone II, steady reactive-diffusive layer (finite-rate chemistry).

The dependent variables are nondimensionalized as

$$\rho = \frac{\rho^*}{\rho^*_\infty} \qquad u = \frac{u^* r^*_s}{D^*_{T,\infty}} \qquad p = \frac{p^*}{\rho^*_\infty R^* T^*_\infty}$$
$$Y_O = \frac{Y^*_O}{\sigma} \qquad Y_F = \frac{Y^*_F}{Le_F} \qquad \theta = \frac{c^*_p(T^* - T^*_\infty)}{Q^*} \tag{1}$$

The characteristic length is taken to be r^*_s, and the characteristic droplet lifetime t^*_d and the characteristic diffusion time t^*_g are, respectively, taken to be

$$t^*_d = \frac{\rho^*_l}{\rho^*_\infty}\frac{r^{*2}_{s,i}}{D^*_{T,\infty}} \qquad t^*_g = \frac{r^{*2}_s}{D^*_{T,\infty}} \tag{2}$$

In terms of this characteristic length and time, nondimensional length and time coordinates are defined as

$$x = r^*/r^*_s \qquad t = t^*/t^*_g \qquad \tau = t^*/t^*_d \tag{3}$$

For sufficiently subcritical conditions, ρ^*_l is much larger than ρ^*_∞, which results in $t^*_d \gg t^*_g$, so that the effect of droplet surface regression is negligible in investigating the combustion characteristics over the characteristic diffusion time t^*_g.

Prior to introducing the conservation equations, it is convenient to define coupling functions as[10]

$$G \equiv \theta + Y_O \qquad Z \equiv Y_F - Y_O \tag{4}$$

Use of these coupling functions enables us to write the conservation equations for total energy and fuel, free of the chemical reaction term. The conservation equations for mass, oxidizer, fuel, and energy are thus written, respectively, as

$$\frac{\partial \rho}{\partial t} + \frac{1}{x^2}\frac{\partial m}{\partial x} = 0 \tag{5}$$

$$\mathcal{L}_O(Y_O) = -w \tag{6}$$

$$\mathcal{L}_F(Z) = \left(\frac{1}{Le_F} - 1\right)\left(\rho\frac{\partial Y_O}{\partial t} + \frac{m}{x^2}\frac{\partial Y_O}{\partial x}\right) \tag{7}$$

$$\mathcal{L}_T(G) = \frac{\gamma - 1}{\gamma q}\frac{\partial p}{\partial t} \tag{8}$$

where the differential operator $\mathcal{L}_i$ is defined as

$$\mathcal{L}_i \equiv \rho\frac{\partial}{\partial t} + \frac{m}{x^2}\frac{\partial}{\partial x} - \frac{1}{Le_i}\frac{1}{x^2}\frac{\partial}{\partial x}\left(\rho D_T x^2 \frac{\partial}{\partial x}\right) \qquad i = O, F, T \tag{9}$$

with $Le_O = Le_T = 1$. The chemical source term in Eq. (6) is given by

$$w = DaY_OY_Fe^{-E^*/R^*T^*} \tag{10}$$

where the Damköhler number is defined as $Da \equiv Le_F B^*(r_s^{*2}/D_{T,\infty}^*)$, which is proportional to the square of the droplet radius. The frequency factor B^* is taken to be proportional to p^n with a typical value of the pressure exponent n lying between 0 and 2. From the assumption preceding Eq. (1), $\rho D_T = [1+q(G-Y_O)]^a$, and typically $a \approx \frac{3}{4}$. Finally, the equation of the state is

$$p = \rho[1+q(G-Y_O)] \tag{11}$$

The boundary conditions for Eqs. (5–8) are

$$\begin{aligned} x = 1{:}\ \rho D_T \frac{\partial Y_{Os}}{\partial x} &= m\left(Y_O - \sigma^{-1}\right) \\ \rho D_T \frac{\partial Z}{\partial x} &= m\left[Le_F Z_s - (1-Le_F)Y_{Os} + \sigma^{-1}\right] \\ \rho D_T \frac{\partial G}{\partial x} &= m\left(L + Y_{Os} - \sigma^{-1}\right) \\ G &= Y_{Os} + \theta_s \end{aligned} \tag{12}$$

$$x \to \infty{:}\ Y_O \to 0 \quad Z \to 1/Le_F \quad G \to 0$$

For a monochromatic pressure oscillation with a small oscillation amplitude ε, the pressure p can be expressed in complex notation as

$$p = 1 + \varepsilon e^{i\omega t} + \cdots \tag{13}$$

where the nondimensional frequency is $\omega \equiv \omega^* r_s^{*2}/D_{T,\infty}^*$. Given the oscillating pressure, the reaction-sheet location x_f is expected to respond as

$$x_f = \bar{x}_f + \varepsilon \tilde{x}_f e^{i\omega t} + \cdots \tag{14}$$

where $\tilde{x}_f$ is the complex amplitude of the reaction-sheet oscillation. Because profiles of the dependent variables, such as θ, Y_i, ρ, and m, are functions of the independent coordinate x and the parameter x_f, any dependent variable $\mathcal{F}$ is also expanded in a form

$$\mathcal{F}(x; x_f) = \bar{\mathcal{F}}(x; \bar{x}_f) + \varepsilon e^{i\omega t}[\tilde{\mathcal{F}}(x; \bar{x}_f) + \tilde{x}_f \hat{\mathcal{F}}(x; \bar{x}_f)] + \cdots \tag{15}$$

where $\hat{\mathcal{F}}(x; x_f) \equiv \partial \bar{\mathcal{F}}/\partial x_f$. The term involving $\tilde{\mathcal{F}}$ represents the direct influence of the oscillatory pressure, whereas the term involving $\tilde{x}_f \hat{\mathcal{F}}$ represents the indirect effect that arises through oscillation of the reaction sheet. Substituting the expansions into Eqs. (5–12) and collecting the terms of the same orders in ε, we obtain the governing equations and boundary conditions for the mean field as well as those for the acoustic field.

Mean-Field Structure

The mean-field conservation equations for the convective–diffusive layer, obtained from time averaging of Eqs. (5–8), are

$$\bar{\mathcal{L}}_O(\bar{Y}_O) = 0 \qquad \bar{\mathcal{L}}_F(\bar{Z}) = \left(\frac{1}{Le_F} - 1\right)\frac{\bar{m}}{x^2}\frac{d\bar{Y}_O}{dx} \qquad \bar{\mathcal{L}}_T(\bar{G}) = 0 \tag{16}$$

where mass conservation leads to a constant value of $\bar{m}$, an eigenvalue of the system. Time averaging of Eq. (11) gives the mean equation of the state as

$$1 = \bar{\rho}[1+q(\bar{G}-\bar{Y}_O)] \tag{17}$$

The averaged differential operator $\bar{\mathcal{L}}_i$ from Eq. (9) is

$$\bar{\mathcal{L}}_i \equiv \frac{\bar{m}}{x^2}\frac{d}{dx} - \frac{1}{Le_i}\frac{1}{x^2}\frac{d}{dx}\left(\frac{x^2}{\bar{\rho}^a}\frac{d}{dx}\right) \qquad i = O, F, T \tag{18}$$

where use has been made of Eqs. (4) and (17) to yield $\overline{\rho D_T} = 1/\bar{\rho}^a$. The boundary conditions are identical to those of Eq. (12) if all variables $\mathcal{F}$, including ρD_T and L, are replaced by $\bar{\mathcal{F}}$.

Because σ for H_2–LOX flames is large (typically 8), the reaction sheet is located close to the oxidizer boundary, resulting in a larger heat loss to the oxidizer side of the reaction sheet. Under these conditions, leakage of the fuel through the reaction zone occurs because the chemical reaction associated with fuel consumption rapidly freezes in the oxidizer stream. For this type of flame structure, Liñán's premixed-flame regime,[5] in which fuel leaks through the reaction sheet by an amount of order unity, while the oxidizer is completely consumed at order unity, provides a more accurate description of the flame structure than does the more conventional diffusion-flame regime. Therefore, the convective–diffusive layer is analyzed with a constraint that $Y_O = 0$ for $x > x_f$.

In the reactive–diffusive layer, appropriate stretched variables are defined by

$$\phi = \beta Y_O/G_f \qquad \xi = A\beta(x - x_f) \tag{19}$$

where the large parameter of expansion is the Zel'dovich number. The Zel'dovich number β and the scaling factor A, respectively, are defined by

$$\beta = \frac{qG_f(E^*/R^*T_\infty^*)}{(1+qG_f)^2} \qquad A = -\frac{1}{G_f}\frac{dY_O}{dx}\bigg|_{x=x_f^-} \tag{20}$$

After substituting Eq. (19) into Eq. (6), the inner equation is found at leading order to be

$$2\phi_{\xi\xi} = \Lambda\phi e^{-(\phi+\alpha\xi)} \tag{21}$$

$$\phi_\xi \to 0 \quad \text{as} \quad \xi \to \infty \qquad \phi_\xi \to -1 \quad \text{as} \quad \xi \to -\infty$$

where the reduced Damköhler number Λ and the downstream heat-loss parameter α are

$$\begin{aligned} \Lambda &= \frac{2DaZ_f}{\beta^2 A^2(1+qG_f)^a}\exp\left(-\frac{E^*/R^*T_\infty^*}{1+qG_f}\right) \\ \alpha &= -\frac{1}{AG_f}\frac{dG}{dx}\bigg|_{x=x_f} \end{aligned} \tag{22}$$

Here, Z_f and G_f represent the fuel mass fraction and temperature at the reaction sheet, respectively. For a given value of α, Λ is found as an eigenvalue to be[5]

$$\Lambda \approx 1 - 1.344\alpha + 0.6307\alpha^2 \tag{23}$$

The mean-field structure is solved by a finite volume method. Once a mean reaction-sheet location $\bar{x}_f$ is specified, the subsequent solutions of Eqs. (16) yield the conditions at the reaction sheet. From Eqs. (20), (22), and (23), the Damköhler number Da can be obtained. Resulting variations of the flame temperature, evaporation rate, and reaction-sheet location are shown in Fig. 2 for $T_s^* = 140$ K, $T_\infty^* = 500$ K, $q = 100$, $L = 0.00104$, and $E^*/R^*T_\infty^* = 35$, values selected to corresponds to LOX droplet condition under some rocket-chamber conditions. We also chose $a = 0$ and $Le_F = 1.0$

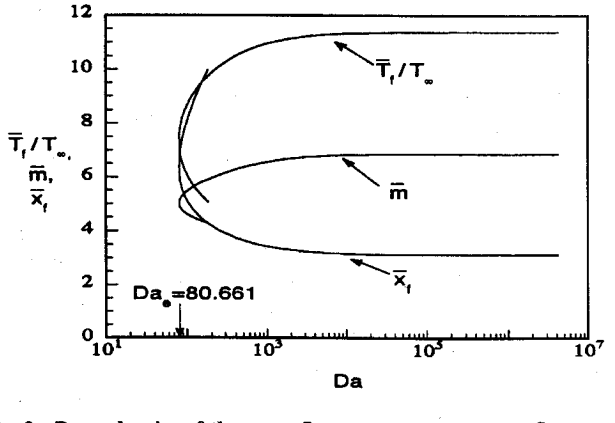

Fig. 2 Dependencies of the mean flame temperature, mass flow rate, and reaction-sheet location on the Damköhler number with q = 100, T_s^* = 140 K, p^* = 2.8 MPa, and $E^*/R^*T_\infty^*$ = 35.

for simplicity in these numerical calculations; the influences of temperature-dependent thermal conductivity and of nonunity fuel Lewis number are discussed later. The reaction-sheet location $\bar{x}_f = 3.1296$ corresponds to the Burke–Schumann limit, i.e., $Da \to \infty$, in which the mean evaporation rate $\bar{m}$ is maximum. As Da decreases with decreasing droplet diameter, the reaction sheet moves away from the droplet surface, and the fuel begins to leak toward the droplet. Excessive leakage of the fuel results in the extinction, which can be identified by the turning point in Fig. 2. In this case, which corresponds to $\beta = 4.11$, extinction of the flame is observed at $\bar{x}_f = 6.395$, $\bar{T}_f^*/T_\infty^* = 7.35$, $\bar{m} = 5.018$, and $Da_e = 80.661$.

Acoustic-Field Structure

The conservation equations for the acoustic field in the convective–diffusive zones are

$$\frac{1}{x^2}\frac{\mathrm{d}\tilde{m}}{\mathrm{d}x} + i\omega(\tilde{\rho} + \tilde{x}_f\hat{\rho}) = 0 \tag{24}$$

$$\bar{\mathcal{L}}_O(\tilde{Y}_O) + \tilde{\mathcal{L}}_O(\bar{Y}_O) + i\omega\bar{\rho}\,(\tilde{Y}_O + \tilde{x}_f\hat{Y}_O) = 0 \tag{25}$$

$$\bar{\mathcal{L}}_F(\tilde{Z}) + \tilde{\mathcal{L}}_F(\bar{Z}) + i\omega\bar{\rho}(\tilde{Z} + \tilde{x}_f\hat{Z}) = \left(\frac{1}{Le_F} - 1\right) \times \left[\frac{\tilde{m}}{x^2}\frac{\mathrm{d}\bar{Y}_O}{\mathrm{d}x} + \frac{\bar{m}}{x^2}\frac{\mathrm{d}\tilde{Y}_O}{\mathrm{d}x} + i\omega\bar{\rho}\,(\tilde{Y}_O + \tilde{x}_f\hat{Y}_O)\right] \tag{26}$$

$$\bar{\mathcal{L}}_T(\tilde{G}) + \tilde{\mathcal{L}}_T(\bar{G}) + i\omega\bar{\rho}\,(\tilde{G} + \tilde{x}_f\hat{G}) = i\omega[(\gamma - 1)/\gamma q] \tag{27}$$

$$\tilde{\rho} = \bar{\rho}[1 - q\bar{\rho}(\tilde{G} - \tilde{Y}_O)] \tag{28}$$

where the differential operator $\tilde{\mathcal{L}}_i$ is

$$\tilde{\mathcal{L}}_i \equiv \frac{\tilde{m}}{x^2}\frac{\mathrm{d}}{\mathrm{d}x} - \frac{1}{Le_i}\frac{1}{x^2}\frac{\mathrm{d}}{\mathrm{d}x}\left[x^2\frac{aq(\tilde{G} - \tilde{Y}_O)}{\bar{\rho}^{a-1}}\frac{\mathrm{d}}{\mathrm{d}x}\right] \qquad i = O, F, T \tag{29}$$

The boundary conditions for the acoustic field are found to be

$$\begin{aligned}
x = 1\text{:}\quad & \frac{1}{\bar{\rho}^a}\frac{\mathrm{d}\tilde{Y}_O}{\mathrm{d}x} + \frac{aq(\tilde{G} - \tilde{Y}_O)}{\bar{\rho}^{a-1}}\frac{\mathrm{d}\bar{Y}_O}{\mathrm{d}x} \\
& = \tilde{m}_s\left(\bar{Y}_{Os} - \sigma^{-1}\right) + \bar{m}\tilde{Y}_{Os} \\
& \frac{1}{\bar{\rho}^a}\frac{\mathrm{d}\tilde{Z}}{\mathrm{d}x} + \frac{aq(\tilde{G} - \tilde{Y}_O)}{\bar{\rho}^{a-1}}\frac{\mathrm{d}\bar{Z}}{\mathrm{d}x} \\
& = \tilde{m}_s\left[Le_F\tilde{Z}_s - (1 - Le_F)\tilde{Y}_{Os} + \sigma^{-1}\right] \\
& + \bar{m}[Le_F\tilde{Z}_s - (1 - Le_F)\tilde{Y}_{Os}] \\
& \frac{1}{\bar{\rho}^a}\frac{\mathrm{d}\tilde{G}}{\mathrm{d}x} + \frac{aq(\tilde{G} - \tilde{Y}_O)}{\bar{\rho}^{a-1}}\frac{\mathrm{d}\bar{G}}{\mathrm{d}x} \\
& = \tilde{m}_s\left(\bar{Y}_{Os} - \sigma^{-1} + \tilde{L}\right) + \bar{m}(\tilde{Y}_{Os} + \tilde{L}) \\
& \tilde{G} = \tilde{Y}_{Os} + \tilde{\theta}_s \\
x \to \infty\text{:}\quad & \tilde{Y}_O = 0 \quad \tilde{Z} = 0 \quad \tilde{G} = (\gamma - 1)/\gamma q
\end{aligned} \tag{30}$$

where $\tilde{L}$ and $\tilde{\theta}_s$ are the rates at which the logarithms of the latent heat and of the saturation temperature vary with respect to the logarithm of the saturation pressure and $\tilde{L} = -0.000628$ and $\tilde{\theta}_s = 0.000455$ for LOX at $p^* = 2.8$ MPa.

To obtain the solutions for the acoustic field, the mean field and its derivatives with respect to x_f must be known for a given value of $\bar{x}_f$. The governing equations and the boundary conditions for these derivatives are given in the Appendix. To close the system for the acoustic field, it is necessary to determine the acoustic response of the reaction-sheet location $\tilde{x}_f$ by considering the response of the reactive–diffusive layer. Because the characteristic reaction time is small compared with the characteristic acoustic time, the reaction-zone analysis, based on quasisteadiness of the reactive–diffusive layer, is still valid. The acoustic response of the reaction sheet can be obtained by linearized perturbations of the matching conditions coming from the outer convective–diffusive layer.

As a first step, a field variable $\mathcal{F}$ at the instantaneous reaction sheet x_f is expanded about the mean reaction sheet $\bar{x}_f$:

$$\mathcal{F}|_{x_f} = \bar{\mathcal{F}}(\bar{x}_f; \bar{x}_f) + \varepsilon e^{i\omega t}[\tilde{\mathcal{F}}(\bar{x}_f; \bar{x}_f) + \tilde{x}_f\breve{\mathcal{F}}(\bar{x}_f; \bar{x}_f)] + \cdots \tag{31}$$

where $\breve{\mathcal{F}}|_{\bar{x}_f}$ is the total derivative of $\bar{\mathcal{F}}|_{x_f}$ with respect to x_f, defined as $\breve{\mathcal{F}}|_{\bar{x}_f} \equiv \mathrm{d}\bar{\mathcal{F}}/\mathrm{d}x_f|_{\bar{x}_f} = \hat{\mathcal{F}}|_{\bar{x}_f} + \bar{\mathcal{F}}_x|_{\bar{x}_f}$. Substituting all of the variables, expanded as shown in Eq. (31), into Eq. (22), the fractional change of the Damköhler number at order ε is found to be

$$\delta Da/Da = \varepsilon e^{i\omega t}[\tilde{\Delta} + \tilde{x}_f\breve{\Delta}] + O(\varepsilon^2) \tag{32}$$

where the two contributions for the fractional variation of the Damköhler number are

$$\begin{aligned}
\tilde{\Delta} = {} & \frac{\bar{\alpha}}{\bar{\Lambda}}\frac{\mathrm{d}\bar{\Lambda}}{\mathrm{d}\bar{\alpha}}\left(\frac{\tilde{G}_x|_{\bar{x}_f}}{\bar{G}_x|_{\bar{x}_f}} - \frac{\tilde{Y}_{Ox}|_{\bar{x}_f^-}}{\bar{Y}_{Ox}|_{\bar{x}_f^-}}\right) + 2\frac{\tilde{Y}_{Ox}|_{\bar{x}_f^-}}{\bar{Y}_{Ox}|_{\bar{x}_f^-}} - \frac{\tilde{Z}|_{\bar{x}_f}}{\bar{Z}|_{\bar{x}_f}} \\
& + (a - 4)\frac{q\tilde{G}|_{\bar{x}_f}}{1 + q\bar{G}|_{\bar{x}_f}} - \tilde{\beta}\bar{G}|_{\bar{x}_f} \\
\breve{\Delta} = {} & \frac{\bar{\alpha}}{\bar{\Lambda}}\frac{\mathrm{d}\bar{\Lambda}}{\mathrm{d}\bar{\alpha}}\left(\frac{\breve{G}_x|_{\bar{x}_f}}{\bar{G}_x|_{\bar{x}_f}} - \frac{\breve{Y}_{Ox}|_{\bar{x}_f^-}}{\bar{Y}_{Ox}|_{\bar{x}_f^-}}\right) + 2\frac{\breve{Y}_{Ox}|_{\bar{x}_f^-}}{\bar{Y}_{Ox}|_{\bar{x}_f^-}} - \frac{\breve{Z}|_{\bar{x}_f}}{\bar{Z}|_{\bar{x}_f}} \\
& + (a - 4)\frac{q\breve{G}|_{\bar{x}_f}}{1 + q\bar{G}|_{\bar{x}_f}} - \tilde{\beta}\breve{G}|_{\bar{x}_f}
\end{aligned} \tag{33}$$

Because $B^* \sim p^n$, $\delta Da/Da = \varepsilon e^{i\omega t}n$, thereby yielding the jump condition

$$\tilde{\Delta} + \tilde{x}_f\breve{\Delta} = n \tag{34}$$

to close the acoustic-field problem. The method parallels that of our earlier work.[4]

Results and Discussion

General characteristics of the reaction-sheet response can be best seen from the well-known S-curve behavior, shown in Fig. 2. The reaction-sheet location x_f is plotted there as a function of Da. If acoustic pressure oscillations are superimposed on the steady flame, the reactivity will increase with increasing pressure, thereby resulting in an increase of Da. The reaction sheet then migrates to a location with a smaller value of x_f, at which the oxidizer mass flux $Y_{Ox}(x_f^-)$ is larger, and the fuel leakage Z_f is smaller. As seen from Fig. 2, for the same fractional amount of variation of the Damköhler number, $\delta Da/Da$, the displacement of the reaction sheet is much larger for near-extinction flames than for near-equilibrium flames because of the rapid variation of the reaction-sheet location near the turning point.

Detailed results of the calculation are shown in Fig. 3 for the real part of the oscillation amplitude of the reaction sheet, $Re(\tilde{x}_f)$, as a function of Da for several values of ω. In Fig. 3, the aforementioned behavior of $\tilde{x}_f$ is best seen in the case with smaller ω ($\omega = 0.1$). Near extinction, the value of $\tilde{x}_f$ moves to a larger negative value. On the other hand, the variation appears to be more gradual for larger ω because the larger unsteady accumulation effect associated with the terms involving $i\omega\tilde{x}_f$ in Eqs. (24–27) impedes the reaction-sheet response. Note that, in the near-equilibrium regime, $\tilde{x}_f$ has small positive values for small ω. Near equilibrium, the effect of finite-rate chemistry is no longer dominant. Instead, variation of the latent heat with pressure becomes more important. As pressure increases, the latent heat of LOX decreases, thereby leading to increased mass flux m. Then the reaction sheet will be pushed away from the droplet surface, so that $Re(\tilde{x}_f)$ becomes positive. For larger ω, the reaction sheet fails to respond immediately to the variation of the mass flux

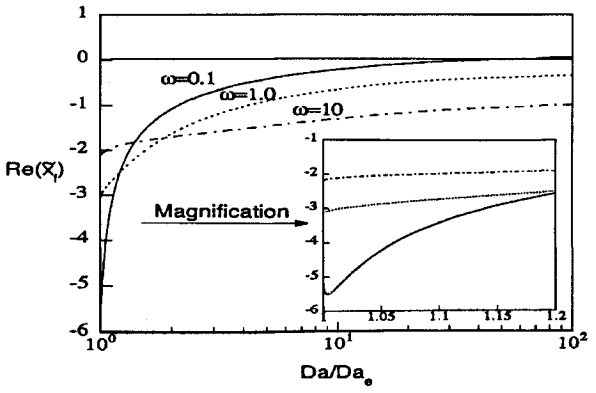

Fig. 3 Variations of the real parts of the reaction-sheet oscillations for various nondimensional acoustic frequencies with the same conditions as Fig. 2 and $n = 1$, $\gamma = 1.2$.

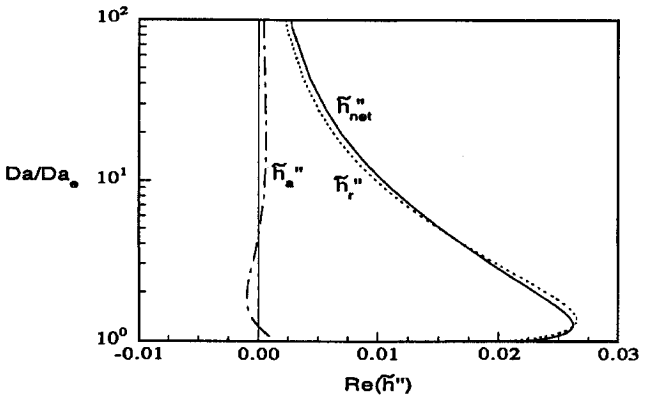

Fig. 4 Dependencies of the heat-release-rate oscillations per unit reaction-surface area on the Damköhler number at $\omega = 1.0$ for conditions of Fig. 3.

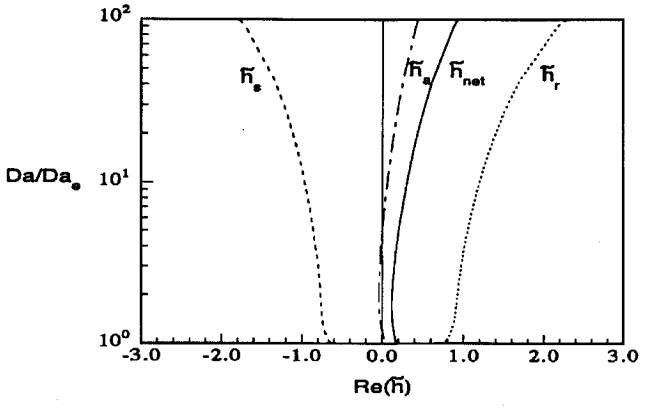

Fig. 5 Dependencies of the heat-release-rate oscillations per droplet flame on the Damköhler number at $\omega = 1.0$ for conditions of Fig. 3.

at the reaction sheet, and $Re(\tilde{x}_f)$ consequently exhibits a negative value.

The Rayleigh criterion[11] indicates that acoustic amplification occurs if, on the average, heat is added in phase with the pressure increase during the oscillation. To further investigate the Rayleigh criterion, we consider the rate of heat release H^* measured per droplet as

$$H^* = -4\pi r_f^{*2} Q^* \rho^* D_O^* \left.\frac{\partial Y_O}{\partial r^*}\right|_{r_f^{*-}}$$

$$= -4\pi\, Q^* \rho_\infty^* D_{T,\infty}^* r_{se}^* \left(\frac{Da}{Da_e}\right)^{\frac{1}{2}} x_f^2 (1+qG_f)^a Y_{Ox}|_{x_f^-} \quad (35)$$

where the relationships $r_f^* = r_s^* x_f$, $Da/r_s^{*2} = Da_e/r_{se}^{*2}$, and $\rho^* D_O^*|_{r_f^*} = \rho_\infty^* D_{T,\infty}^* (1+qG_f)^a$ are used in obtaining the second equality. Upon expanding $H^* = \bar{H}^* + \varepsilon e^{i\omega t}\tilde{H}^*$, comparison with Eq. (35) leads to $\tilde{H}^*$ as

$$\tilde{H}^* = 4\pi Q^* \rho_\infty^* D_{T,\infty}^* r_{se}^* (\tilde{h}_a + \tilde{h}_r + \tilde{h}_s) \quad (36)$$

where

$$\tilde{h}_a = -\bar{x}_f^2 \left(\frac{Da}{Da_e}\right)^{\frac{1}{2}} (1+q\bar{G}_f)^a \bar{Y}_{Ox}|_{\bar{x}_f^-} \left(\frac{\tilde{Y}_{Ox}|_{\bar{x}_f^-}}{\bar{Y}_{Ox}|_{\bar{x}_f^-}} + \frac{aq\tilde{G}_f}{1+q\bar{G}_f}\right)$$

$$\tilde{h}_r = -\bar{x}_f^2 \left(\frac{Da}{Da_e}\right)^{\frac{1}{2}} (1+q\bar{G}_f)^a \bar{Y}_{Ox}|_{\bar{x}_f^-} \left(\frac{\check{Y}_{Ox}|_{\bar{x}_f^-}}{\bar{Y}_{Ox}|_{\bar{x}_f^-}} + \frac{aq\check{G}_f}{1+q\bar{G}_f}\right)\tilde{x}_f \quad (37)$$

$$\tilde{h}_s = -\bar{x}_f^2 (Da/Da_e)^{\frac{1}{2}} (1+q\bar{G}_f)^a \bar{Y}_{Ox}|_{\bar{x}_f^-} (2\tilde{x}_f/\bar{x}_f)$$

$$\tilde{h}_{\text{net}} = \tilde{h}_a + \tilde{h}_r + \tilde{h}_s$$

Here, $\tilde{h}_a$ is the normalized rate of heat-release fluctuation originating from the acoustic fluctuation of the field variables, $\tilde{h}_r$ is that originating from variation of the oxidizer mass flux by the reaction-sheet oscillation, and $\tilde{h}_s$ is that originating from the reactive-area variation.

Prior to discussing the results for the $\tilde{h}$, it is useful to get an insight into the underlying physical processes by comparing with the previous results for strained diffusion flames,[4] in which oscillation of the rate of heat release is measured per unit reaction-surface area. Figure 4 shows these nondimensional quantities per unit reaction-surface area as

$$\tilde{h}_a'' = \frac{Da_e}{\bar{x}_f^2 Da}\tilde{h}_a \qquad \tilde{h}_r'' = \frac{Da_e}{\bar{x}_f^2 Da}\tilde{h}_r \qquad \tilde{h}_{\text{net}}'' = \tilde{h}_a'' + \tilde{h}_r'' \quad (38)$$

The component associated with the reactive-area variation does not appear in this comparison. The response component directly associated with the acoustic field, i.e., $\tilde{h}_a''$, exhibits only a slight variation throughout the entire range of the Damköhler number. On the other hand, the other response component associated with the reaction-sheet oscillation, i.e., $\tilde{h}_r''$, rapidly increases and becomes the dominant response near extinction, which is consistent with the response characteristics of strained diffusion flamelets.

However, if the heat-release response is considered per droplet, i.e., if the complete $\tilde{h}$ is considered, droplet flames exhibit quite different characteristics from strained diffusion flames because the reaction-surface area varies proportionally to the Damköhler number. The response characteristics per droplet flame are shown in Fig. 5. Contrary to Fig. 4, the flame responses now decrease in magnitude as the flame approaches extinction because the total reaction-surface area decreases with decreasing Damköhler number. Although the reaction-sheet standoff ratio, x_f, increases with decreasing Da, the droplet radius r_s^* decreases much faster, causing the total reaction-surface area to decrease almost in proportion to Da. In addition, the response component associated with the reaction-surface area variation, i.e., $\tilde{h}_s$, cancels most of the amplification effect arising from the response associated with the reaction-sheet oscillation, $\tilde{h}_r$. As the reaction sheet moves to the droplet surface to respond to higher reactivity during the period of higher acoustic pressure, the oxidizer gradient increases to produce an amplification effect, indicated by $\tilde{h}_r$, but the accompanying decrease of the reaction-sheet area gives rise to an attenuation contribution to cancel $\tilde{h}_r$. Consequently, the net flame response remains small and nearly constant.

This conclusion does not, however, imply that near-extinction conditions, created by making the spray finer, are not conducive to acoustic instability. If the total combustion response is measured per reactant mass consumed, then a finer spray produces a larger combustion response, which is, however, smaller than the flame response coming from the strained diffusion flame consuming an equal amount of oxidizer.

For hydrocarbon–LOX systems, the situation is quite different because the flame would surround fuel rather than oxidizer droplets.

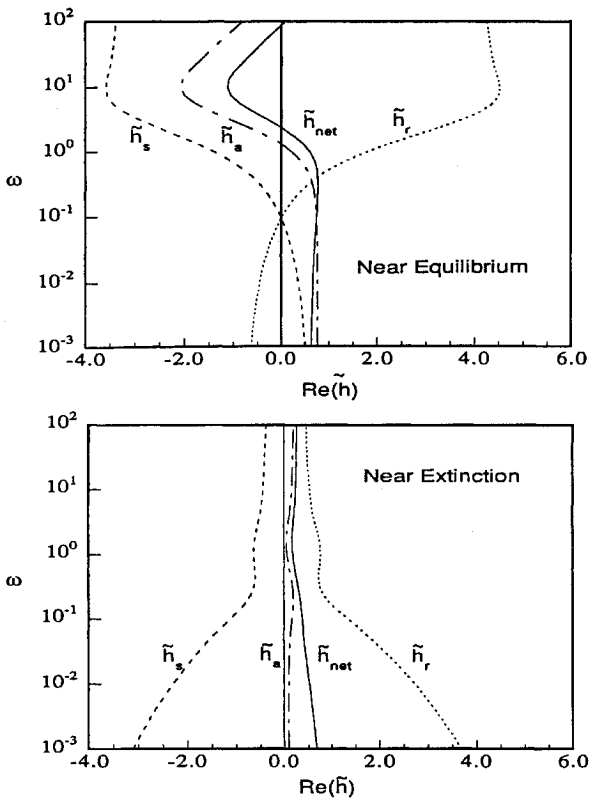

Fig. 6 Dependencies of the heat-release-rate oscillations per droplet flame on the nondimensional acoustic frequency for a near-equilibrium condition (Da/Da_e = 43.3) and for a near-extinction condition (Da/Da_e = 1.01) for conditions of Fig. 3.

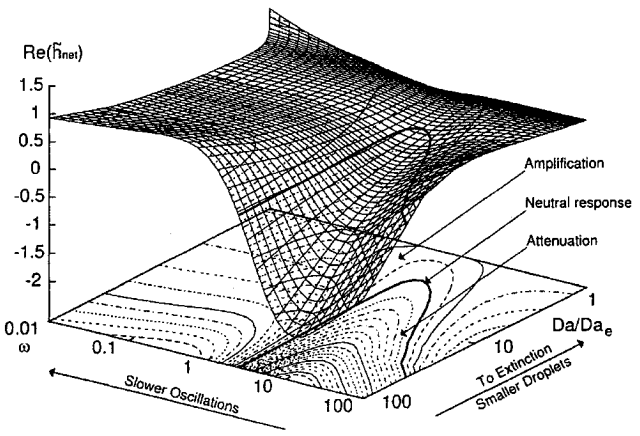

Fig. 7 Variation of the net response of heat-release rate with the Damköhler number and the nondimensional acoustic frequency for conditions of Fig. 3. The isoscalar contours are marked for every 0.1 change in $Re(\tilde{h}_{net})$.

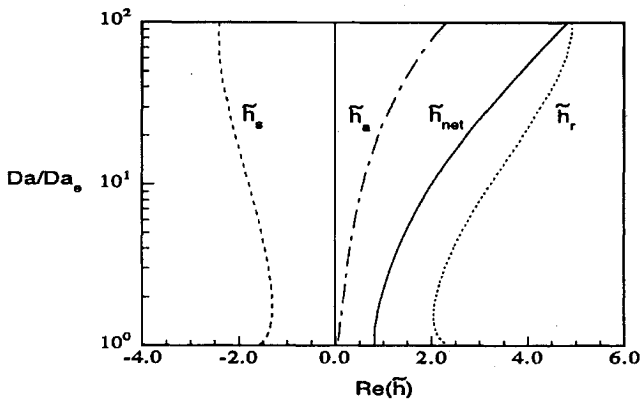

Fig. 8 Dependencies of the heat-release-rate oscillations per droplet flame on the Damköhler number at $\omega = 1.0$ for $Le_F = 0.6$ and $a = 0.75$ with other conditions corresponding to those of Fig. 3.

The AEA theory predicts that the reaction sheet moves toward the oxidizer boundary at infinity, resulting in an amplification by flame-area increase. However, the AEA analysis would be misleading for hydrocarbon–LOX systems because it would predict fuel leakage through the reaction sheet, whereas, opposite to hydrogen–LOX droplet flames, leakage of the oxidizer is predicted from the analysis adopting full and reduced chemical kinetics.[12] Therefore, the $\tilde{h}_s$ term also contributes to attenuation for hydrocarbon–LOX systems. However, the net amount of combustion response is anticipated to remain small because the parametric range of the stoichiometric mixture fraction for hydrocarbon–oxygen flames falls farther into the diffusion-flame regime of AEA,[5] in which displacement of the reaction sheet is limited to order β^{-1} compared with displacement in the premixed-flame regime. Therefore, oscillation of the reaction sheet may not be a dominant effect for the hydrocarbon–LOX system.

In Fig. 6, variations of the real parts of $\tilde{h}$ are shown as a function of ω for near-equilibrium and near-extinction conditions. For both cases, the net combustion responses closely follow variations of $\tilde{h}_a$ because the effects of $\tilde{h}_r$ and $\tilde{h}_s$ cancel. For the near-equilibrium case, an amplification effect is found in the region of small ω, which most likely arises from the increased evaporation rate $\tilde{m}$ associated with the reduced latent heat $\tilde{L}$. For the near-extinction case, the real part of the net heat-release response is small and nearly constant for the entire range of ω. The results for the near-equilibrium case here would be compared with those of Strahle because both cases correspond to $Da \to \infty$. However, the existence of an additional effect $\tilde{h}_s$ makes comparison difficult. Instead, an extensive comparison of Strahle's results with those obtained by AEA can be found in our previous work.[4] Finally, the overall variation of $Re(\tilde{h}_{net})$ is shown as a function of ω and Da in Fig. 7. At low ω or near extinction, an amplification effect exists with a small value of $Re(\tilde{h}_{net})$, whereas attenuation is found at moderate ω and near equilibrium.

Additional numerical results are presented in the remaining figures to examine the influences of nonunity fuel Lewis number and temperature-dependent thermal conductivity. When a representative fuel Lewis number is chosen for zone III, care must be taken because the average molecular weight increases by an order of magnitude, and the thermal conductivity and Lewis number for hydrogen decrease with the inverse of the square root of the average molecular weight as hydrogen approaches the reaction sheet. The Lewis number for hydrogen at the hydrogen boundary is approximately 1.2, whereas that at the reaction sheet is 0.4 because the average molecular weight is 9 times larger at the reaction sheet than at the hydrogen boundary. The mean Lewis number for zone III is estimated as 0.6 by harmonic averaging. Harmonic averaging is more appropriate because the rate of mass diffusion is proportional to the inverse of the Lewis number. The dependence of the Lewis number on temperature is insignificant. Characteristics of the droplet flame are more strongly dependent on the thermal conduction in zone I than in zone III. The temperature exponent a for ρD_T is thus taken to be 0.75 from a typical value for oxygen.

The numerical results for $Le_F = 0.6$ and $a = 0.75$ are shown in Figs. 8 and 9. Variations of the heat-release responses per droplet with Da are shown in Fig. 8. Although each contribution, $\tilde{h}_a$, $\tilde{h}_r$, and $\tilde{h}_s$, exhibits a behavior similar to that in Fig. 5, one notable difference is that the magnitude of $Re(\tilde{h}_r)$ is now somewhat larger than that of $Re(\tilde{h}_s)$. After adding these two contributions associated with the reaction-sheet oscillations, there exists a moderate amplification contribution that arises mainly from the increase of the diffusion coefficient by shifting x_f to where the temperature is higher. Therefore, the net heat-release response is larger for the conditions of Fig. 8 than for those of Fig. 5. However, the heat-release response for the droplet flame still will be smaller than that for the strained flame because the effect of the reaction-surface reduction is still operative. Figure 9 shows the various contributions to the heat-release response as functions of ω for near-extinction and near-equilibrium conditions. Although each term behaves in a qualitatively similar manner to the corresponding term in Fig. 6, there

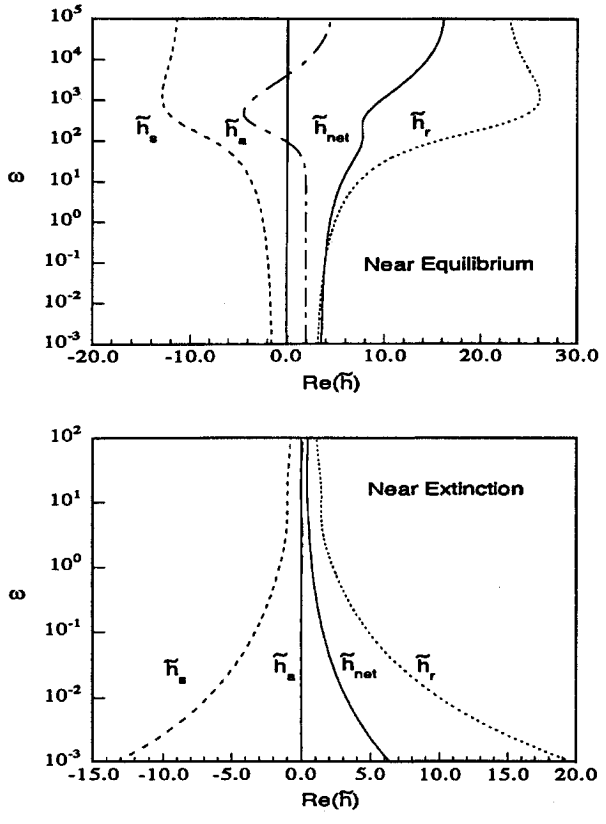

Fig. 9 Dependencies of the heat-release-rate oscillations per droplet flame on the nondimensional acoustic frequency for a near-equilibrium condition ($Da/Da_e = 73.8$) and for a near-extinction condition ($Da/Da_e = 1.0001$) for $Le_F = 0.6$ and $a = 0.75$ with other conditions corresponding to those of Fig. 3.

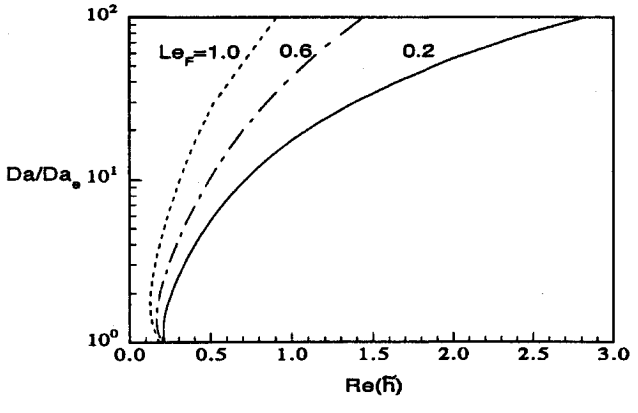

Fig. 10 Effects of the nonunity fuel Lewis number on the fluctuations of the net heat-release rate as functions of the Damköhler number at $\omega = 1.0$ for conditions of Fig. 3.

are quantitative differences. Increase of the diffusivity and decrease of the reaction-sheet location relatively diminish the unsteady-accumulation effect, so that a larger value of ω is required to exhibit the distinctive behavior. Near equilibrium, the entire range of ω now corresponds to amplification, whereas a small attenuation region was found for moderate ω in Fig. 6. The disappearance of the attenuation region is a result of the additional amplification effect arising from variation of the diffusivity associated with the reaction-sheet oscillation. A test calculation with $Le_F = 0.6$ and $a = 0$ exhibited an attenuation region near $\omega = 10$, supporting this explanation. Near extinction, the dominant responses are $\tilde{h}_r$ and $\tilde{h}_s$, both associated with the reaction-sheet oscillation, and the net amplification is only somewhat larger than that in Fig. 6.

Additional results showing influence of nonunity fuel Lewis numbers on the net flame response is shown in Fig. 10 for various values of Le_F. If nonunity Lewis number of the ambient hydrogen gas is considered, the reaction sheet moves toward the droplet surface because of the increased rate of hydrogen diffusion into the reaction sheet. The greater oxidizer mass flux into the reaction sheet results in a larger net flame response for smaller values of Le_F. Although not shown here, the contributions of $\tilde{h}_a$, $\tilde{h}_r$, and $\tilde{h}_s$ to $\tilde{h}_{\text{net}}$ have behaviors similar to those explained earlier, so that the preceding conclusions concerning canceling effects are not modified qualitatively by the values of a and Le_F.

Conclusion

The acoustic pressure response of H_2–LOX flames was analyzed for spherical subcritical droplet flames by extending the premixed-flame regime analysis of AEA previously employed in the acoustic-response analysis for strained diffusion flames. The reaction sheet of the droplet flame behaved in a manner similar to that of the strained diffusion flames. However, the net flame response for the droplet flames is much smaller than that for the strained diffusion flames because oscillations of the reaction sheet cause a reduction of the reaction-surface area, thereby giving an additional attenuation mechanism. Although the spherical-droplet-flame model is not realistic under the presence of strong convective effects, this analysis nevertheless is expected to provide many generally valid characteristics of the acoustic responses of convective droplet flames. The attenuation effect associated with the reaction-surface variation still will be present in convective droplet flames.

In addition to the paper's conclusion that strained diffusion flamelets produce larger contributions to overall acoustic responses in motors, the applicability of the droplet-flamelet model to acoustic instabilities is further limited by experimental observations suggesting that the strained diffusion flamelet model may be more relevant as a microscopic flame model for turbulent spray flames in liquid-propellant rocket engines. Although there are no conclusive experiments determining whether flames near the injectors are composed of strained diffusion flamelets enveloping the spray or of individual droplet flamelets, a visualization of LOX–H_2 flames, taken in a single-element coaxial-injector test rocket, shows flamelets surrounding the LOX spray jet rather than surrounding the droplets. The LOX spray appears to be too dense to support individual droplet flamelets because penetration of the gaseous fuel into the LOX spray is insufficient.

Appendix: Calculation of Mean-Field Derivatives

To determine the influence of the oscillation of the reaction sheet, we must calculate various derivatives of the mean field with respect to x_f. Because the details of the procedure are discussed by Kim and Williams,[4] only an outline of the aspects unique to the present problem is given here. By differentiating Eq. (16), the governing equations for the partial derivatives are found to be

$$\bar{\mathcal{L}}_O(\hat{Y}_O) + \hat{\mathcal{L}}_O(\bar{Y}_O) = 0 \tag{A1}$$

$$\bar{\mathcal{L}}_T(\hat{G}) + \hat{\mathcal{L}}_T(\bar{G}) = 0 \tag{A2}$$

$$\bar{\mathcal{L}}_F(\hat{Z}) + \hat{\mathcal{L}}_F(\bar{Z}) = \left(\frac{1}{Le_F} - 1\right)\left(\frac{\bar{m}}{x^2}\frac{d\hat{Y}_O}{dx} + \frac{\hat{m}}{x^2}\frac{d\bar{Y}_O}{dx}\right) \tag{A3}$$

where the differential operator $\hat{\mathcal{L}}_i$ and the boundary conditions are identical to those of Eqs. (29) and (30), respectively, with the tilde replaced by a circumflex except for $\hat{G} = \hat{Y}_{Os}$ and $\hat{G} = 0$. The corresponding equation of the state is

$$\hat{\rho} = -q\bar{\rho}^2\hat{\theta} \tag{A4}$$

Because the gradient of $\bar{Y}_O$ is discontinuous at the reaction sheet, differentiation of $\bar{Y}_O$ will give rise to a discontinuity in $\hat{Y}_O$. From continuity of Y_O, we find the jump conditions for $\hat{Y}_O$ to be

$$\hat{Y}_O(\bar{x}_f^-; \bar{x}_f^-) = -\bar{Y}_{Ox}(\bar{x}_f^-; \bar{x}_f^-) \qquad \hat{Y}_O(\bar{x}_f^+; \bar{x}_f^+) = 0 \tag{A5}$$

On the other hand, if $a = 0$ and $Le_F = 1.0$, profiles of G and Z are independent of the reaction-sheet location and are continuously differentiable throughout the whole domain; no jump conditions for

$\hat{G}$ and $\hat{Z}$ are necessary. However, if $a \neq 0$ or $Le_F \neq 1.0$, discontinuities for $\hat{G}$ and $\hat{Z}$ appear for their gradients because $\bar{G}$ and $\bar{Z}$ are continuous only up to first derivatives. Integrating Eqs. (A2) and (A3) across the reaction sheet, the jump conditions for $\hat{G}_x$ and $\hat{Z}_x$ are found to be

$$\hat{G}_x(\bar{x}_f^+; \bar{x}_f^+) - \hat{G}_x(\bar{x}_f^-; \bar{x}_f^-) = a\bar{\rho}q\bar{G}_x(\bar{x}_f; \bar{x}_f)\bar{Y}_{Ox}(\bar{x}_f^-; \bar{x}_f^-) \quad \text{(A6)}$$

$$\hat{Z}_x(\bar{x}_f^+; \bar{x}_f^+) - \hat{Z}_x(\bar{x}_f^-; \bar{x}_f^-) = \left[a\bar{\rho}q\bar{Z}_x(\bar{x}_f; \bar{x}_f) + (Le_F - 1)\bar{\rho}^a(\bar{m}/\bar{x}_f^2)\right]\bar{Y}_{Ox}(\bar{x}_f^-; \bar{x}_f^-) \quad \text{(A7)}$$

From the above jump conditions, it is seen again that there are no discontinuities for $\hat{G}_x$ and $\hat{Z}_x$ if $a = 0$ and $Le_F = 1.0$. Finally, note that there are no jumps of $\bar{G}$ and $\bar{Z}$ because the uniform acoustic pressure field does not introduce a differential operation.

Acknowledgments

This research has been supported by the U.S. Air Force Office of Scientific Research through AFOSR Grant F49620-94-1-0166 and by the Turbo and Power Machinery Research Center at Seoul National University.

References

[1]Harrje, D. J., and Reardon, F. H. (eds.), *Liquid Propellant Rocket Instability*, NASA SP-194, 1972.

[2]Yang, V., and Anderson, W. E. (eds.), *Liquid Rocket Engine Combustion Instability*, Vol. 169, Progress in Astronautics and Aeronautics, AIAA, Washington, DC, 1995.

[3]Strahle, W. C., "Periodic Solutions to a Convective Droplet Burning Problem: The Stagnation Point," *10th Symposium (International) on Combustion*, Combustion Inst., Pittsburgh, PA, 1965, pp. 1315–1325.

[4]Kim, J. S., and Williams, F. A., "Contribution of Strained Diffusion Flames to Acoustic Pressure Response," *Combustion and Flame*, Vol. 98, No. 3, 1994, pp. 279–299.

[5]Liñán, A., "The Asymptotic Structure of Counterflow Diffusion Flames for Large Activation Energies," *Acta Astronautica*, Vol. 4, 1974, pp. 1007–1039.

[6]Balakrishnan, G., Treviño, C., and Mauss, F., "The Asymptotic Structure of Hydrogen-Air Diffusion Flames," *Combustion and Flame*, Vol. 91, Nos. 3, 4, 1992, pp. 246–256.

[7]Clavin, P., and Lazimi, D., "Theoretical Analysis of Oscillatory Burning of Homogeneous Solid Propellant Including Non-Steady Gas Phase Effects," *Combustion Science and Technology*, Vol. 83, Nos. 1–3, 1992, pp. 1–32.

[8]Kim, J. S., and Williams, F. A., "Boundaries of Acoustic Instability in Liquid-Propellant Rocket Engines: A Theoretical Explanation of an Empirical Correlation," *Journal of Propulsion and Power*, Vol. 12, No. 3, 1996, pp. 621–624.

[9]Card, J. M., and Williams, F. A., "Asymptotic Analysis with Reduced Chemistry for the Burning of *n*-Heptane Droplets," *Combustion and Flame*, Vol. 91, No. 2, 1992, pp. 187–199.

[10]Liñán, A., and Williams, F. A., *Fundamental Aspects of Combustion*, Oxford Univ. Press, New York, 1993, pp. 144–146.

[11]Rayleigh, J. W. S., *The Theory of Sound*, Vol. 2, Dover, New York, 1945, pp. 226–235.

[12]Seshadri, K., and Peters, N., "Asymptotic Structure and Extinction of Methane-Air Diffusion Flames," *Combustion and Flame*, Vol. 73, No. 1, 1988, pp. 23–44.